



# Organic acid-assisted preparation of highly dispersed Co/ZrO<sub>2</sub> catalysts with superior activity for CO<sub>2</sub> methanation

Wenhui Li<sup>a</sup>, Yi Liu<sup>a</sup>, Minchen Mu<sup>a</sup>, Fanshu Ding<sup>a</sup>, Zhongmin Liu<sup>b</sup>, Xinwen Guo<sup>a,\*</sup>,  
Chunshan Song<sup>a,c,\*\*</sup>

<sup>a</sup> State Key Laboratory of Fine Chemicals, PSU-DUT Joint Center for Energy Research, School of Chemical Engineering, Dalian University of Technology, Dalian 116024, PR China

<sup>b</sup> National Engineering Laboratory for Methanol to Olefins, Dalian National Laboratory for Clean Energy, Dalian Institute of Chemical Physics, Chinese Academy of Sciences, Dalian 116023, PR China

<sup>c</sup> Clean Fuels & Catalysis Program, EMS Energy Institute, PSU-DUT Joint Center for Energy Research, Departments of Energy and Mineral Engineering and Chemical Engineering, The Pennsylvania State University, University Park, PA 16802, USA

## ARTICLE INFO

### Keywords:

CO<sub>2</sub> methanation  
Cobalt catalyst  
ZrO<sub>2</sub>  
Organic acid  
High dispersion

## ABSTRACT

Various organic acids were investigated for preparing the highly dispersed cobalt catalysts on zirconia support, Co/ZrO<sub>2</sub>, by an acid-assisted incipient wetness impregnation. The organic acid-assisted preparation results in highly dispersed Co/ZrO<sub>2</sub> catalysts which demonstrate superior catalytic activity with only 2 wt.% Co loading for CO<sub>2</sub> methanation. Among the acids, the carboxylic acids with bigger molecular weight, more carboxyl groups and hydroxyl groups are more effective. Furthermore, the amino acids can also change the charge property of ZrO<sub>2</sub> surface through controlling the solution pH and increase the metal dispersion through strong electrostatic adsorption. It is worth mentioning that, among the numerous organic acids, citric acid-assisted preparation gives Co/ZrO<sub>2</sub> catalyst with superior catalytic activity and increased the CO<sub>2</sub> conversion from 38% to 85% with highest turnover frequency. The linear relationship between metal dispersion and TOF with the molar ratio of acid to cobalt  $n_{CA/Co}$  ranging from 0 to 2 demonstrates the importance of well dispersed metal particles in the enhanced activity. However, when the  $n_{CA/Co}$  value exceeds 2 and the metal particle size further decreases, but no further enhancement is observed and the CO<sub>2</sub> conversion even slightly decreased at the  $n_{CA/Co}$  value of 5. The organic acids-assisted strategy can lead to increased metal dispersion and higher TOF for Co/ZrO<sub>2</sub> catalysts; the appropriate metal dispersion corresponds to the suitable Co-ZrO<sub>2</sub> interaction with oxygen vacancy which leads to more catalytically active sites for CO<sub>2</sub> adsorption and catalytic hydrogenation. The organic acid-assisted strategy provides a new design approach for highly dispersed and active catalysts.

## 1. Introduction

Continuing consumption of fossil fuels worldwide led to an increasing CO<sub>2</sub> concentration in the atmosphere. Mitigation of CO<sub>2</sub> emission into atmosphere is in urgent need due to the continuing rise in atmospheric CO<sub>2</sub> concentration (e.g., exceeding 410 ppm in 2017 [1]) and its negative impact on the climate system. On the other hand, CO<sub>2</sub> can be used as an energy carrier for the transformation of renewable energy. Methane (CH<sub>4</sub>), a product of CO<sub>2</sub> hydrogenation, is the main component of liquefied natural gas (LNG), which has been widely used in the combustion systems. The so-called “power to gas” (PtG) concept has garnered significant attention recently [2,3], in which CO<sub>2</sub> reacts

with H<sub>2</sub> produced by water electrolysis with electricity generated using renewable (wind or solar) energy, to produce CH<sub>4</sub> as an alternative source of natural gas. In addition, in the ammonia synthesis and fuel cell systems, methanation can be used to prevent catalyst poisoning through the elimination of CO from H<sub>2</sub>-rich gas flow [4].

CO<sub>2</sub> methanation can be catalyzed by transition metals such as Co [5–8], Ni [9,10], Ru [11,12], Rh [13] and Pd [14,15] and when they are supported on the metal oxide Al<sub>2</sub>O<sub>3</sub> [16,17], SiO<sub>2</sub> [18,19], ZrO<sub>2</sub> [20], TiO<sub>2</sub> [21,22], CeO<sub>2</sub> [23] and zeolites [9]. Our recent experiments for CO<sub>2</sub> methanation reveal that Co catalysts supported on ZrO<sub>2</sub> show superior activity for CO<sub>2</sub> methanation without deactivation after 300 h time on stream (TOS) compared with the Co catalysts supported on

\* Corresponding author.

\*\* Corresponding author at: Clean Fuels & Catalysis Program, EMS Energy Institute, PSU-DUT Joint Center for Energy Research, Departments of Energy and Mineral Engineering and of Chemical Engineering, The Pennsylvania State University, University Park, PA, 16802, USA.

E-mail addresses: [guoxw@dlut.edu.cn](mailto:guoxw@dlut.edu.cn) (X. Guo), [csong@psu.edu](mailto:csong@psu.edu) (C. Song).

<https://doi.org/10.1016/j.apcatb.2019.05.028>

Received 24 February 2019; Received in revised form 2 May 2019; Accepted 7 May 2019

Available online 08 May 2019

0926-3373/ © 2019 Elsevier B.V. All rights reserved.

other supports [24]. Re-dispersion of Co species on the ZrO<sub>2</sub> support during reduction by H<sub>2</sub> was observed by STEM/EDS. New Co-Zr phase formed on the Co-ZrO<sub>2</sub> interface was directly observed by TEM for the first time. The oxygen vacancies on the ZrO<sub>2</sub> detected by XPS may help to activate CO<sub>2</sub> and H<sub>2</sub>O and resist deactivation. In conjunction with experimental work, we performed density functional theory (DFT) calculations to gain mechanistic insight into the support effect over Co/ZrO<sub>2</sub> for CO<sub>2</sub> methanation [25]. DFT results uncovered an energetically more favorable H<sub>2</sub> dissociative adsorption, faster H\* surface migration, and more facile CoO reduction (Co-O bond cleavage) on Co/ZrO<sub>2</sub> than on Co/Al<sub>2</sub>O<sub>3</sub>, thus rationalizing the experimentally observed lower temperature and higher degree of cobalt oxide reduction on the ZrO<sub>2</sub> support. In addition, the CO<sub>2</sub> species prefer to adsorb on Co-ZrO<sub>2</sub> interface. The present work builds on the previous study and attempts to provide more Co-ZrO<sub>2</sub> interface by reducing Co particle size with a higher level of Co dispersion on ZrO<sub>2</sub>.

Reducing particle size of metals is an effective approach to increase the metal-support interface; consequently, enormous efforts have been devoted to preparing ultra-small nanoparticles (NPs) and increasing metal dispersion [12,26–28]. In addition, the activity and selectivity of these supported catalysts were also sensitive to the chemical state of active sites tuned by the interaction between the active metals and oxide supports [10,29–31]. Ma et al. [32] have prepared Ir/CeO<sub>2</sub> catalysts with various Ir particle sizes using ligand-free method, and tested these in CO<sub>2</sub> methanation. Their results suggest that, the chemical state of Ir could be finely tuned by altering the loading of the metal. The metal-support interaction affects the chemical state of active metal on the supports and further affects the activity. Indeed, the modification of the chemical state, for instance the oxidation state of the metal catalyst [33], could influence the adsorption behavior of the reactants and the subsequent conversion of the reaction intermediates, and thus the reaction path. However, only a limited number of recent studies have addressed tailoring of the catalytic activity of supported base metals in a given reaction by tuning the particle size and then the chemical state of the base metal NPs.

Developing a facile and efficient strategy to prepare highly dispersed Co-ZrO<sub>2</sub> catalyst is desirable. It was previously demonstrated that the pyrolysis of metal complexes was an effective method for synthesizing highly dispersed catalysts [34–37]. However, the ligands are costly. Therefore, it is highly desirable to find a low-cost and general strategy to prepare highly dispersed supported Co catalyst for CO<sub>2</sub> methanation. Organic acids, as the low-cost compounds, with the carboxyl at the end, may be used to act as a complexing agent due to its complexation of COO<sup>-</sup> and Co<sup>2+</sup> [38]. Different organic acids play discrepant role on account of the molecular weight, structure and any other functional groups such as hydroxyl and amino groups. In this work, we examined the use of organic acids with different molecular weight, carboxyl, hydroxyl and amidogen for preparing highly dispersed Co catalysts supported on ZrO<sub>2</sub>. This work led us to develop a new strategy for the organic acid-assisted synthesis of highly active Co-ZrO<sub>2</sub> catalysts for CO<sub>2</sub> methanation. The citric acid-assisted preparation of catalysts with superior activity was investigated in detail. Different amounts of citric acid were added to the impregnation solutions complexed with Co ions [38] to increase the Co dispersion and decrease the metal particle size on the ZrO<sub>2</sub>. The activity has been increased more than 2 times on the prepared catalyst compared with the catalyst prepared by conventional method shown in our recent work [24] with an average turnover frequency (TOF) reaching 1,116 mol of carbon dioxide per mole of cobalt per hour. The metal particle size decreased with the increasing amount of citric acid added; however, the catalytic activity did not increase with the decreasing metal particle size in a linear fashion. We have explored the reasons for the high activity catalysts through XRD, TEM, CO<sub>2</sub>-TPD, H<sub>2</sub>-TPR, and XPS characterizations and insight was gained regarding the structure-property relationships for the Co/ZrO<sub>2</sub> catalyst. It was concluded that the chemical state and catalytic activity of Co species can be tuned by varying the size of Co

NPs supported on ZrO<sub>2</sub>. This work also provide reference for highly dispersed Co-based CO<sub>2</sub> methanation catalysts design with appropriate metal-support interaction.

## 2. Experimental section

### 2.1. Catalyst preparation

Nano monoclinic ZrO<sub>2</sub> was used as the support materials. ZrO<sub>2</sub> samples were prepared by dissolving ZrO(NO<sub>3</sub>)<sub>2</sub>·2H<sub>2</sub>O (> 45% ZrO<sub>2</sub>, Aladdin Chemicals) in a mixture (ca. 70 ml) of urea (> 99%, Aladdin Chemicals) and deionized water, followed by thermal treatment in a Teflon-lined stainless-steel autoclave (ca. 100 ml) at 160 °C under autogenous pressure for 20 h. The concentration of Zr<sup>4+</sup> in the solution was 0.4 M, and the urea/ Zr<sup>4+</sup> molar ratio was 10. The resulting precipitate was washed thoroughly with water and dried at 110 °C overnight in ambient air and then calcined at 400 °C for 4 h in dry air [39]. Co/ZrO<sub>2</sub> catalysts were prepared by the impregnation using aqueous or ethanol solution of Co(NO<sub>3</sub>)<sub>2</sub>·6H<sub>2</sub>O (> 99%, Aladdin Chemicals) and one of the following organic acid: propionic acid, malonic acid, succinic acid, adipic acid, L-malic acid, L-tartaric acid, n-hexylic acid, citric acid, L-alanine and L-lysine. The Co loading was fixed at 2 wt%, and the molar ratio of organic acid to Co was kept at 2. For citric acid, we conducted a more detailed study with the molar ratios of citric acid to Co varied at 0.1, 0.5, 1, 2 and 5. The impregnated samples were dried at 120 °C for 12 h and calcined at 500 °C for 4 h with heating rate at 2 °C min<sup>-1</sup> in air. The citric acid (CA)-assisted catalysts are denoted as (xCA)-Co/ZrO<sub>2</sub>, where x represents the molar ratio of citric acid to Co.

### 2.2. Catalytic test

The catalytic hydrogenation of CO<sub>2</sub> was carried out in a pressurized fixed-bed flow reactor (inner diameter 8 mm) loaded with 0.5 g powder catalyst for each test (catalyst bed height 10 mm). Prior to the reaction, the catalyst was pre-reduced in H<sub>2</sub> at 400 °C overnight. After the reduction, the feed gas was switched to the mixture of CO<sub>2</sub> and H<sub>2</sub> with H<sub>2</sub>/CO<sub>2</sub> molar ratio of 4, and the reactor was pressurized to 3 MPa and heated up to 400 °C; the space velocity was 7200 ml g<sup>-1</sup> h<sup>-1</sup>.

The products were analyzed on-line by a gas chromatograph (FULI GC 97). CO<sub>2</sub>, CO and CH<sub>4</sub> were analyzed on a carbon molecular sieve column with a thermal conductivity detector (TCD). The conversion of CO<sub>2</sub> and CH<sub>4</sub> selectivity were calculated as Eqs. (1) and (2):

$$\text{CO}_2 \text{ Conversion}(\%) = \frac{n_{\text{CO}_2, \text{in}} - n_{\text{CO}_2, \text{out}}}{n_{\text{CO}_2, \text{in}}} \times 100\% \quad (1)$$

$$\text{CH}_4 \text{ Selectivity}(\%) = \frac{n_{\text{CH}_4, \text{out}}}{n_{\text{CO}_2, \text{in}} - n_{\text{CO}_2, \text{out}}} \times 100\% \quad (2)$$

where  $n_{\text{CO}_2, \text{in}}$  and  $n_{\text{CO}_2, \text{out}}$  represent the molar concentration of CO<sub>2</sub> in the feed and effluent, respectively;  $n_{\text{CH}_4, \text{out}}$  represents the molar concentration of CH<sub>4</sub> in the effluent.

### 2.3. Characterization of catalysts

Transmission electron microscopy (TEM) images were obtained by using a Tecnai F30 HRTEM instrument (FEI Corp.) at an acceleration voltage of 300 kV. The samples were dispersed into ethanol with ultrasonic treatment for 10 min, and a drop of the suspension was placed on a copper grid for TEM observation.

H<sub>2</sub>-temperature programmed reduction (TPR) was conducted with ChemBETPulsar TPR/TPD equipment (Quantachrome, USA) to analyze the reducibility of the calcined catalysts. Prior to reduction, ~ 0.10 g of the calcined sample was charged into the quartz tube and flushed with high purity Ar at 300 °C for 1 h, followed by cooling down to room temperature. The TPR program was then initiated by switching to 5 vol % H<sub>2</sub>/Ar with a total flow rate of 30 ml min<sup>-1</sup> and heating up to 900 °C

at  $10\text{ }^{\circ}\text{C min}^{-1}$ . A cooling trap was placed before the detector. Dispersion of cobalt particles was determined by  $\text{H}_2$  titration using the same equipment. After following the same procedure of reduction, the gas was changed to high-purity Ar for 1 h, and then allowed to cool down to  $30\text{ }^{\circ}\text{C}$ , followed by  $\text{H}_2$  titration. The cobalt dispersion was estimated based on the assumption of  $\text{H}/\text{Co} = 1$  [40,41] and calculated using Eq. (3):

$$\text{Dispersion (\%)} = \frac{n_{\text{Hads}}}{m_{\text{Co}} \times \text{reduction deg}/M_{\text{Co}}} \times 100\% \quad (3)$$

where  $n_{\text{Hads}}$  represents the adsorbed H atom mole number;  $m_{\text{Co}}$  represents the weight of cobalt in the tested sample;  $M_{\text{Co}}$  represents the molecular weight of cobalt.

$\text{CO}_2$ -temperature programmed desorption (TPD) was conducted (in the same equipment as TPR) with Ar as the carrier gas. About 0.10 g catalyst was charged into the quartz tube and reduced in 5 vol%  $\text{H}_2/\text{Ar}$  (ca.  $30\text{ ml min}^{-1}$ ) at  $400\text{ }^{\circ}\text{C}$  for 2 h. The catalyst bed was subsequently flushed with Ar (ca.  $30\text{ ml min}^{-1}$ ) for 30 min at the same temperature. Then, the sample was cooled down to  $30\text{ }^{\circ}\text{C}$ , followed by  $\text{CO}_2$  flow for 30 min (ca.  $30\text{ ml min}^{-1}$ ). After adsorption, the system was purged with argon gas (ca.  $30\text{ ml min}^{-1}$ ) for 30 min to remove weakly-adsorbed species. The TPD program was initiated by heating up to  $450\text{ }^{\circ}\text{C}$  with a rate of  $10\text{ }^{\circ}\text{C min}^{-1}$ .  $\text{CO}$ -TPD measurement was performed using the same equipment with similar procedure, except  $\text{CO}$  was introduced as probe molecule (ca.  $30\text{ ml min}^{-1}$ ).

X-ray photoelectron spectra (XPS) were measured with a VG ESCALAB250 Spectrometer with a monochromatic Al-K $\alpha$  (1486.6 eV) at 15 kV and 10 mA, and all binding energies were referenced to the C 1s at 284.6 eV. The calcined catalyst precursors were reduced in the fixed-bed reactors under the reaction conditions and then cooled down to room temperature under the hydrogen atmosphere. To avoid the oxidation of the reduced catalysts, passivating treatment was done for the reduced catalysts.

XRD patterns of calcined catalyst precursors and spent catalysts were measured using a Rigaku SmartLab (9) diffractometer with Cu K $\alpha$  radiation ( $\lambda = 1.5406\text{ \AA}$ ) with 0.02 step size over the range between  $5^{\circ}$  and  $80^{\circ}$ .

FT-IR spectra were collected using an EQUINOX-55 Fourier Transform Infrared Spectrometer (BRUKER) by means of the KBr pellet technique. All spectra were taken in the range  $4000\text{--}400\text{ cm}^{-1}$  at a resolution of  $4\text{ cm}^{-1}$ . The spectra of all samples were presented by subtracting the background spectrum.

Zeta potentials of the samples in deionized water were measured using a zeta potential analyzer (ZETASIZER nanoseries Nano-ZS90, Malvern Instruments). The  $\text{ZrO}_2$  nanoparticles ( $< 100\text{ nm}$ ) were dispersed in deionized water and the solution pH was regulated by  $\text{HNO}_3$  and  $\text{NaOH}$ .

The  $\text{N}_2$  adsorption data such as surface area (BET) and pore size distribution (BJH) of the samples were obtained by using a Quantachrome AUTO-SORB-1-MP sorption analyzer at  $77\text{ K}$ . The catalysts were treated in vacuum at  $300\text{ }^{\circ}\text{C}$  for 2 h before the test.

### 3. Results and discussion

#### 3.1. The organic acid-assisted $\text{Co}/\text{ZrO}_2$ catalysts for $\text{CO}_2$ methanation

##### 3.1.1. Effect of organic acid

The design thinking of organic acid-assisted strategy is to enable the spatial separation of Co species on  $\text{ZrO}_2$  surface by complexing Co ions with organic acid which also help to during calcination process. Such a strategy is expected to suppress metal sintering thereof resulting in the enhanced metal dispersion [42,43]. In order to identify suitable complexing agents for cobalt ions, various organic acids have been investigated. To allow for comparison on the same basis, the dicarboxylic acid with different carbon chain lengths were considered first. Malonic acid ( $\text{C}_3\text{H}_4\text{O}_4$ ), succinic acid ( $\text{C}_4\text{H}_6\text{O}_4$ ) and adipic acid ( $\text{C}_6\text{H}_8\text{O}_4$ ) are

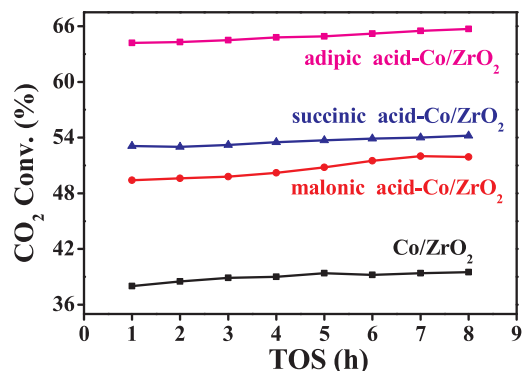


Fig. 1. The catalytic performance of malonic acid, succinic acid and adipic acid assisted  $\text{Co}/\text{ZrO}_2$  catalysts and the benchmark  $\text{Co}/\text{ZrO}_2$  catalyst. Conditions: molar ratio of  $\text{H}_2/\text{CO}_2 = 4/1$ , GHSV =  $7200\text{ ml g}^{-1}\text{ h}^{-1}$ ,  $P = 3\text{ MPa}$ ,  $T = 400\text{ }^{\circ}\text{C}$ .

aliphatic carboxylic acid with two carboxyl groups. The catalysts prepared by dicarboxylic acid-assisted impregnation method were then examined for  $\text{CO}_2$  methanation.

Fig. 1 shows the catalytic performance of the prepared catalysts. Compared with the benchmark  $\text{Co}/\text{ZrO}_2$  catalyst, the dicarboxylic acid addition in the impregnation solution improved the activity of  $\text{Co}/\text{ZrO}_2$  catalysts. The  $\text{CO}_2$  conversion was raised from 38% to 65% and the  $\text{CH}_4$  selectivity stayed at 99% with little change with time over the  $\text{Co}/\text{ZrO}_2$  catalysts. The increased activities with the dicarboxylic acid-assisted  $\text{Co}/\text{ZrO}_2$  catalysts are attributed to the increased metal dispersion caused by the complexation of organic acid and cobalt ions. To examine the anti-sintering effect of organic acid addition, the calcined catalyst precursors were tested by XRD, with a particular focus in the  $2\theta$  range between  $35\text{--}40^{\circ}$ , as presented in Fig. 2. The diffraction peak centered at  $36.8^{\circ}$  on  $\text{ZrO}_2$ -supported catalysts can be attributed to  $\text{Co}_3\text{O}_4$  particles [44], and the intensity is decreased with increasing carbon chain lengths of organic acid, indicating that the  $\text{Co}_3\text{O}_4$  crystallite size is decreased with the increasing carbon chain lengths of organic acid employed.

When a large ligand is added to the impregnation solution, a large complex cluster is formed. As a result of the steric hindrance, the repulsion between adjacent molecules inhibits the aggregation of metal ions. The increase of carbon chain lengths means the steric hindrance

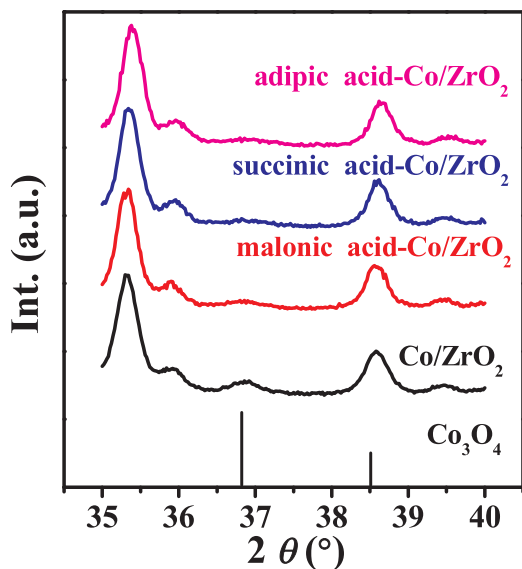


Fig. 2. XRD patterns of calcined catalyst precursors with the malonic acid, succinic acid and adipic acid addition.

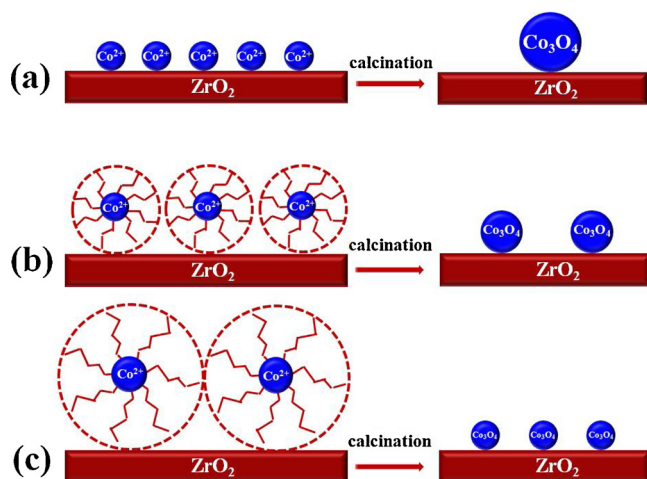


Fig. 3. Metal sintering schematic diagram during calcination process of catalysts precursors prepared by (a) conventional impregnation method, (b) organic acid-assisted impregnation method with relatively shorter carbon chains dicarboxylic acid and (c) organic acid-assisted impregnation method with relatively higher carbon chains dicarboxylic acid.

increase and the increased steric hindrance make the metal particle dispersed better in turn, which is shown as the schematic diagram (Fig. 3). The Co<sub>3</sub>O<sub>4</sub> crystallite size decreased with the increase in carbon chain lengths of the organic acid used; the improved catalytic activity is associated with the increased metal dispersion. Therefore, in the similar chemical environment, the organic acid with higher molecular weight possesses bigger steric hindrance and gives the higher metal dispersion using the complexation of organic acid and cobalt ions.

### 3.1.2. Effect of hydroxyl groups in organic acid

In order to ascertain the hydroxyl group effect, dicarboxylic acids containing different amounts of hydroxyl groups were investigated. Succinic acid (C<sub>4</sub>H<sub>6</sub>O<sub>4</sub>), malic acid (C<sub>4</sub>H<sub>6</sub>O<sub>5</sub>) and tartaric acid (C<sub>4</sub>H<sub>6</sub>O<sub>6</sub>) have no, one and two hydroxyl groups, respectively. The catalysts prepared by hydroxyl acid-assisted impregnation method were examined in CO<sub>2</sub> methanation. The catalytic performance of the prepared catalysts are shown in Fig. 4. Compared with the benchmark Co/ZrO<sub>2</sub> catalyst, the succinic acid addition in the impregnation solution has improved the activity of Co/ZrO<sub>2</sub> catalysts visibly. In particular, the hydroxyl acid further enhanced the catalytic activity. When the acid in the impregnation solution has two hydroxyl groups, the CO<sub>2</sub> conversion increased to the maximum 68%. The XRD patterns (Fig. 5) gave the

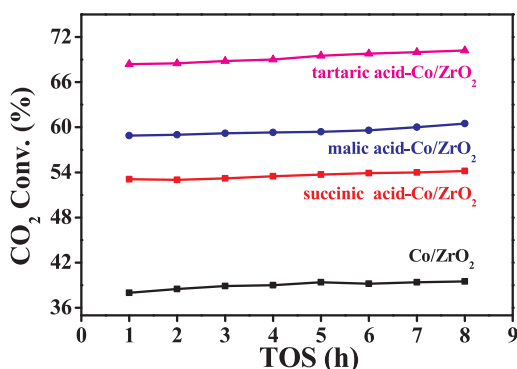


Fig. 4. The catalytic performance of succinic acid, malic acid and tartaric acid-assisted Co/ZrO<sub>2</sub> catalysts and the benchmark Co/ZrO<sub>2</sub> catalyst. Conditions: molar ratio of H<sub>2</sub>/CO<sub>2</sub> = 4/1, GHSV = 7200 ml g<sup>-1</sup> h<sup>-1</sup>, P = 3 MPa, T = 400 °C.

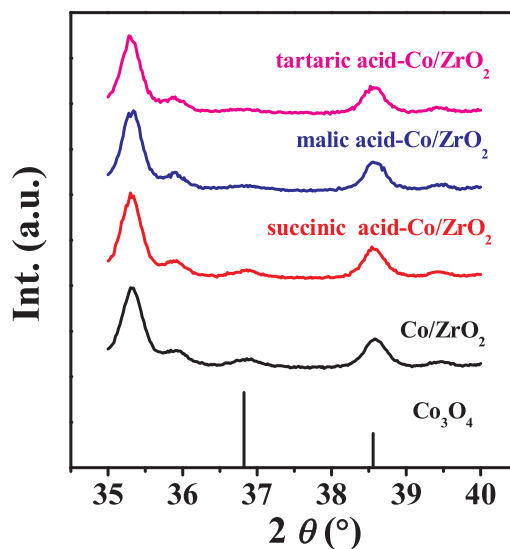


Fig. 5. XRD patterns of calcined catalyst precursors with the succinic acid, malic acid and tartaric acid addition.

evidence of the important role of hydroxyl groups for the metal dispersion. The intensity of diffraction peak associated with Co<sub>3</sub>O<sub>4</sub> decreased with increasing hydroxyl groups in the organic acid, elucidating that the Co<sub>3</sub>O<sub>4</sub> crystallite size is likely to decrease.

The experiments results of succinic acid, malic acid and tartaric acid addition in the impregnation solution illustrate that the hydroxyl group in the organic acid makes a further improvement in the metal dispersion and catalytic performance. According to the literatures [45,46] and the IR spectrum in Fig. 11 (3300 cm<sup>-1</sup>–3400 cm<sup>-1</sup>), there are hydroxyl groups both on the monoclinic and tetragonal ZrO<sub>2</sub> surface. Hydroxyl groups on the surface of oxide materials are known to influence the synthesis of supported metal catalysts [47–50]. Recent evidence suggests that they also influence the stability and dispersion of catalytic nanoparticles [49]. On the contrary, the hydroxyl groups on the Co<sup>2+</sup> clusters also can influence the metal dispersion in turn. One possible reason is that the hydroxyl groups on the Co<sup>2+</sup> clusters can strengthen the interaction between the metal and support through the generation of dehydrating with the ZrO<sub>2</sub> surface hydroxyl groups or interacted with the surface oxygen. Therefore, the hydroxyl group plays the positive role in the synthesis of highly dispersed metal catalysts through organic acid-assisted strategy (Fig. 5).

### 3.1.3. The effect of the amount of carboxyl groups

The essence of organic acid-assisted strategy is the complexation of COO<sup>-</sup> and Co<sup>2+</sup>. Therefore, the amount of carboxyl groups play an important role in the metal dispersion. N-hexylic acid, adipic acid and citric acid, containing 6 carbon atoms with 1, 2 and 3 carboxyl groups, respectively, were selected to confirm the carboxyl groups effect. As the result, the Co<sub>3</sub>O<sub>4</sub> crystallite size decreased (Fig. 7) and the CO<sub>2</sub> conversion increased (Fig. 6) with the increased number of carboxyl groups. Interestingly, the citric acid with three carboxyl groups enhanced the catalytic activity of Co/ZrO<sub>2</sub> catalyst obviously, leading to a significant CO<sub>2</sub> conversion increase from 38% to 85%. The significant improvement of citric acid-assisted Co/ZrO<sub>2</sub> catalyst is attributed to the carboxyl groups primarily. However, the hydroxyl group on the citric acid also has a positive impetus on the metal dispersion, which is in good agreement with the conclusion of hydroxyl groups effect. Consequently, the amount of carboxyl groups of organic acid is an important factor for the acid-assisted strategy; In the similar chemical environment, the more carboxyl groups are the better the catalyst performance is.

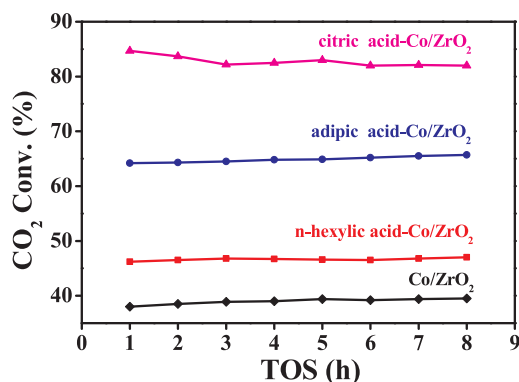


Fig. 6. The catalytic performance of n-hexylic acid, adipic acid and citric acid-assisted Co/ZrO<sub>2</sub> catalysts and the benchmark Co/ZrO<sub>2</sub> catalyst. Conditions: molar ratio of H<sub>2</sub>/CO<sub>2</sub> = 4/1, GHSV = 7200 ml g<sup>-1</sup> h<sup>-1</sup>, P = 3 MPa, T = 400 °C.

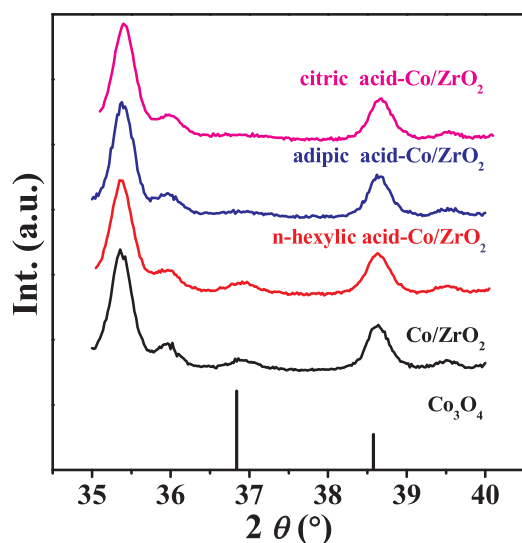


Fig. 7. XRD patterns of calcined catalyst precursors with the n-hexylic acid, adipic acid and citric acid addition.

### 3.1.4. The effect of electrostatic adsorption on the metal dispersion

Amino acids are a branch of organic acids possessing the alkaline amino groups. Propionic acid (C<sub>3</sub>H<sub>6</sub>O<sub>2</sub>), L-alanine (C<sub>3</sub>H<sub>7</sub>O<sub>2</sub>N) and L-lysine (C<sub>6</sub>H<sub>14</sub>O<sub>2</sub>N<sub>2</sub>) were selected to examine the effect of amino group. The catalytic performance of the prepared catalysts are shown in Fig. 8.

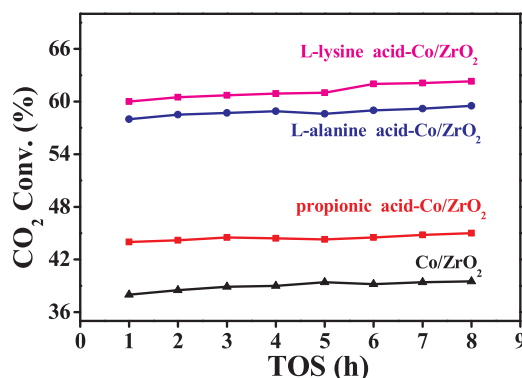


Fig. 8. The catalytic performance of propionic acid, L-alanine and L-lysine-assisted Co/ZrO<sub>2</sub> catalysts and the benchmark Co/ZrO<sub>2</sub> catalyst. Conditions: molar ratio of H<sub>2</sub>/CO<sub>2</sub> = 4/1, GHSV = 7200 ml g<sup>-1</sup> h<sup>-1</sup>, P = 3 MPa, T = 400 °C.

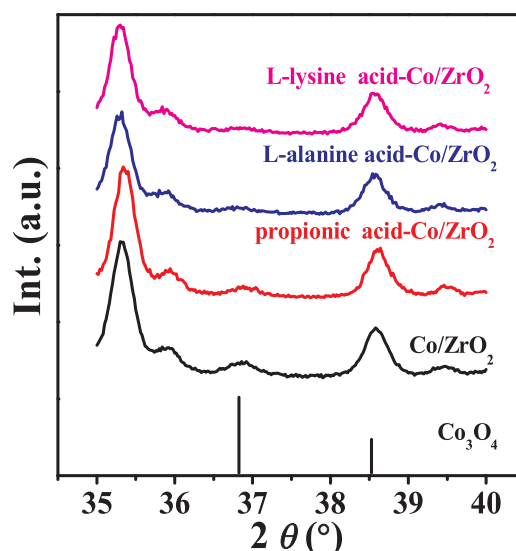


Fig. 9. XRD patterns of calcined catalyst precursors with the propionic acid, L-alanine and L-lysine addition.

Compared with the benchmark Co/ZrO<sub>2</sub> catalyst, the propionic acid addition in the impregnation solution improved the activity of Co/ZrO<sub>2</sub> catalysts due to the increased metal dispersion (Fig. 9) caused by the complexation of COO<sup>-</sup> and Co<sup>2+</sup>. However, the extra alkaline amino group on L-alanine and L-lysine further increased the catalytic activity obviously. Some researchers have made use of the pH shift during impregnation, which can be an important factor in the uptake of metal complexes over support with strong interaction [51,52]. In order to clarify the effect of the alkaline amino group, the pH of the impregnation solution was measured and presented in Table 1. The values of point of zero charge (PZC, pH at which the net charge on metal oxide surface is zero) for ZrO<sub>2</sub> support are shown in Fig. 10. The support surface is positively charged when the pH of the impregnation solution is below the PZC or becomes negatively charged above the PZC value. The amino acid addition in the impregnation solution change the pH from 3.89 to 4.95 and 5.42, which make the positively charged support surface to negatively charged. Regalbuto et al. [53,54] has presented the strategy of strong electrostatic adsorption (SEA) for preparing highly dispersed metals of noble and base metals from ammine complexes over amorphous silica through controlling pH of the impregnation solution. Since the Co<sup>2+</sup> clusters are positively charged, the metal complex might be deposited onto the support surface via strong electrostatic adsorption at pH values above the PZC of ZrO<sub>2</sub>. Therefore, it is also an effective strategy to change the charge property on the support surface through amino acid addition with pH regulation and then increase the metal dispersion through strong electrostatic adsorption.

In short, the organic acid-assisted strategy is effective to synthesis the highly dispersed ZrO<sub>2</sub> supported Co-based catalysts through the complexation of COO<sup>-</sup> and Co<sup>2+</sup>. The general conclusions of the organic acid-assisted strategy for highly dispersed ZrO<sub>2</sub> supported Co-based catalysts are that: the carboxylic acid molecular with larger steric hindrance, more carboxyl groups and hydroxyl groups is the better choice. Furthermore, the amino acids can also change the charge

Table 1  
The pH of the impregnation solution.

Aqueous solution	pH
Co(NO <sub>3</sub> ) <sub>2</sub>	3.89
Co(NO <sub>3</sub> ) <sub>2</sub> + C <sub>3</sub> H <sub>6</sub> O <sub>2</sub>	1.67
Co(NO <sub>3</sub> ) <sub>2</sub> + C <sub>3</sub> H <sub>7</sub> O <sub>2</sub> N	4.95
Co(NO <sub>3</sub> ) <sub>2</sub> + C <sub>6</sub> H <sub>14</sub> O <sub>2</sub> N <sub>2</sub>	5.42

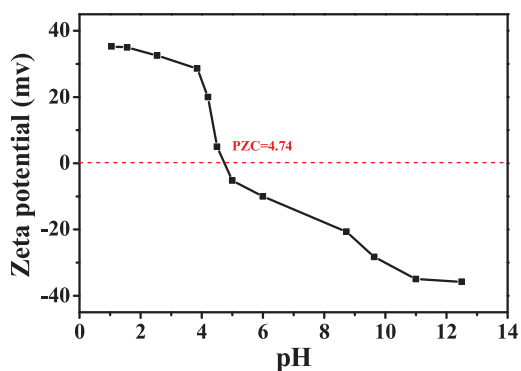


Fig. 10. Effect of pH on the zeta potential of zirconia at room temperature.

property of  $\text{ZrO}_2$  surface through controlling the solution pH and increase the metal dispersion through strong electrostatic adsorption.

It is noteworthy that, among the numerous samples, citric acid-assisted  $\text{Co}/\text{ZrO}_2$  catalyst exhibited the superior catalytic activity and increased the  $\text{CO}_2$  conversion from 38% to 85% which improved more than twice. Therefore, the specific features of the citric acid-assisted  $\text{Co}/\text{ZrO}_2$  catalysts will be discussed in detail below and the effect of citric acid dosage were also investigated.

### 3.2. Physico-chemical properties of citric acid-assisted $\text{Co}/\text{ZrO}_2$ catalysts

CA-Co/ $\text{ZrO}_2$  catalysts prepared with different amounts of citric acid were characterized by FT-IR to investigate the formation of the complex of  $\text{Co}^{2+}$  and citric acid on  $\text{ZrO}_2$ . As benchmark, citric acid, cobalt nitrate, and cobalt citrate, which was the complex of  $\text{Co}^{2+}$  and citric acid, were also measured using FT-IR, as presented in Fig. 11. The spectrum of cobalt citrate exhibits two bands at 1585 and 1417  $\text{cm}^{-1}$ , corresponding to the asymmetric and symmetric vibration of  $\text{RCOO}^-$ , respectively [38]. The band of citric acid with respect to the  $\text{C}=\text{O}$  stretching of carboxyl groups can be observed around 1722  $\text{cm}^{-1}$  [55,56]. Cobalt nitrate displays a band at 1377  $\text{cm}^{-1}$ , which can be attributed to the  $\text{NO}_3^-$  [57,58]. The formation of cobalt citrate on catalyst precursors is evidenced by the increased strength of bands at 1417  $\text{cm}^{-1}$  and 1585  $\text{cm}^{-1}$ , which is further supported by the significant difference in color of the catalyst precursors shown in the Fig. 11 inset photos. When the molar ratio of citric acid to cobalt increases stepwise from 0 to 2, the band at 1377  $\text{cm}^{-1}$  associated with

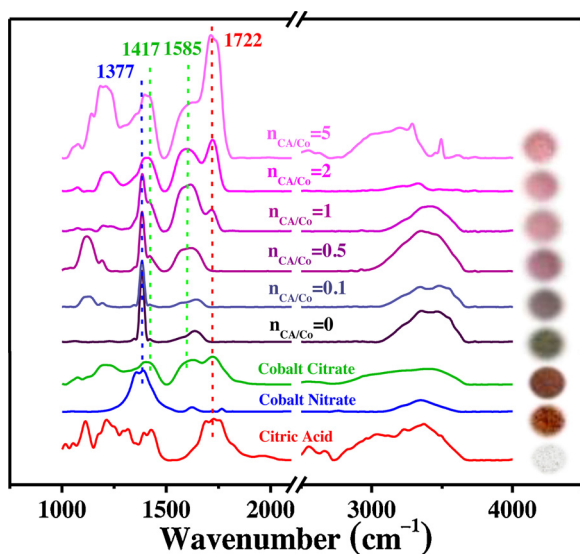


Fig. 11. FT-IR spectra of citric acid, cobalt nitrate, cobalt citrate and catalysts precursors before calcination. Insets are photos of corresponding samples.

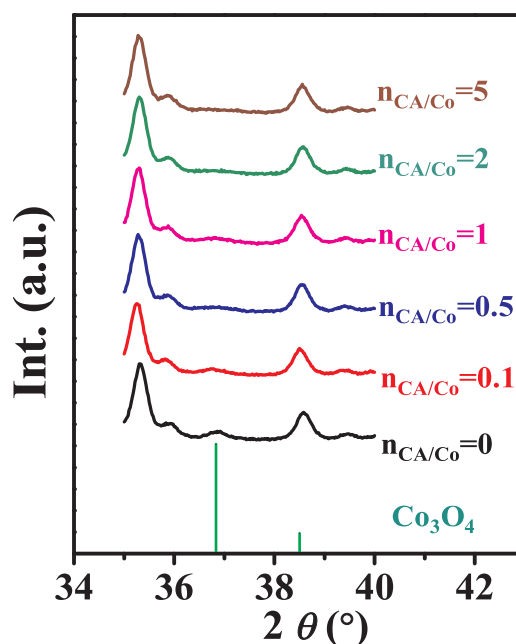


Fig. 12. XRD patterns of calcined catalyst precursors zirconia-supported cobalt catalysts with different concentrations of citric acid addition.

$\text{NO}_3^-$  becomes weaker gradually and even disappears at last. With increasing content of citric acid, the band centered at 1722  $\text{cm}^{-1}$  increased visibly. Hence, citric acid with twice the amount of cobalt ion is sufficient to complex with cobalt ions. The formation of the complex of  $\text{Co}^{2+}$  and citric acid is demonstrated by FT-IR characterization, which is consistent with the design strategy.

To clarify if citric acid addition enhanced the anti-sintering, the calcined catalyst precursors were tested by XRD, with a particular focus in the  $2\theta$  range between 35–40°, as presented in Fig. 12. The diffraction peak centered at 36.8° on  $\text{ZrO}_2$ -supported catalysts can be attributed to  $\text{Co}_3\text{O}_4$  particles [44], and the intensity is decreased with increasing citric acid addition, indicating that the  $\text{Co}_3\text{O}_4$  crystallite size decreased with the increasing content of citric acid. High-resolution TEM was carried out to determine the  $\text{Co}_3\text{O}_4$  particle size distribution, metal particle morphology, and  $\text{Co}_3\text{O}_4$  crystal lattice of CA- $\text{Co}_3\text{O}_4/\text{ZrO}_2$  and  $\text{Co}_3\text{O}_4/\text{ZrO}_2$  samples.

From the particle size distribution histograms shown in the insets of Fig. 13(a-1), (b-1), and (c-1), the mean  $\text{Co}_3\text{O}_4$  particle sizes of OCA, 2CA, and 5CA-assisted  $\text{Co}_3\text{O}_4/\text{ZrO}_2$  are 19 nm, 14 nm and 12 nm, respectively, evidently substantiating the citric acid addition enhanced dispersion of  $\text{Co}_3\text{O}_4$  on  $\text{ZrO}_2$  support. With amplified image of representative particles in Fig. 13(a-2), (b-2), and (c-2), the lattice spacing values are measured, which correspond to the (111) plane of  $\text{Co}_3\text{O}_4$ . The TEM images further confirm the enhancing effect of the cobalt citrate complex used, which is consistent with the results obtained from XRD. The promoting effect in  $\text{Co}_3\text{O}_4$  particle dispersion may result from the stereo-hindrance effect of the cobalt citrate complex as proposed in Fig. 3 and the anchoring effect from the hydroxyl group on the cobalt clusters. The  $\text{N}_2$  adsorption data of support  $\text{ZrO}_2$ , original  $\text{Co}/\text{ZrO}_2$  and citric acid-assisted  $\text{Co}/\text{ZrO}_2$  catalysts have been offered in Table S1. The  $\text{N}_2$  adsorption data show no micropores on zirconia and acid-assisted catalysts and the total pore volume is contributed by the intergranular space. Acid treatment did not improve specific surface area or change the physical properties of catalysts obviously. Therefore, the improved metal dispersion of acid-assisted catalysts is not associated with the higher surface area or the smaller pores. The high dispersion of organic acid-assisted Co-based catalysts is due to the complexation of  $\text{COO}^-$  and  $\text{Co}^{2+}$ .

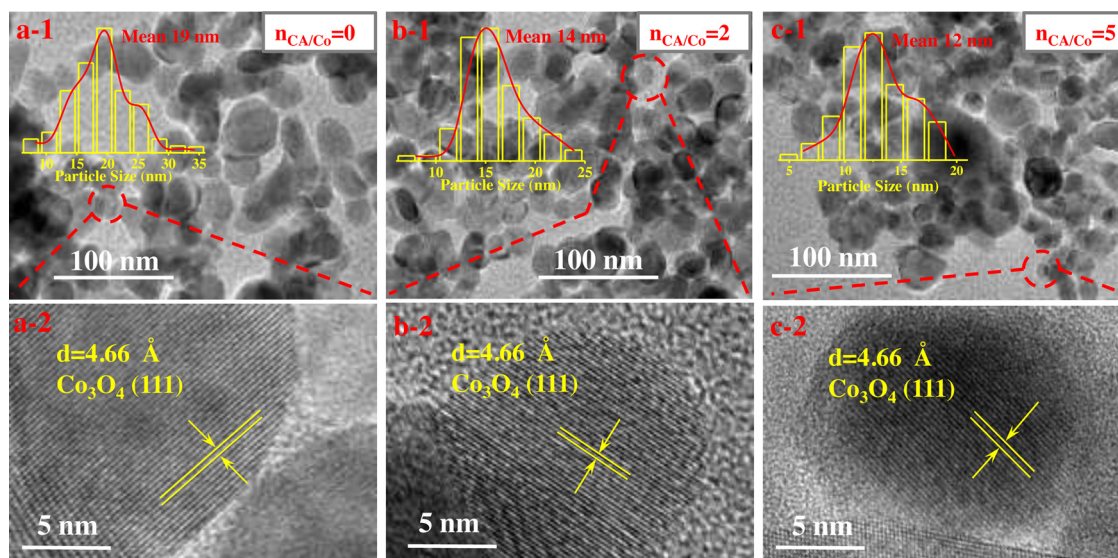


Fig. 13. TEM images of calcined catalyst precursors (a-1, b-1, c-1) 0CA-Co<sub>3</sub>O<sub>4</sub>/ZrO<sub>2</sub>, 2CA-Co<sub>3</sub>O<sub>4</sub>/ZrO<sub>2</sub>, and 5CA-Co<sub>3</sub>O<sub>4</sub>/ZrO<sub>2</sub>, respectively, and (a-2, b-2, c-2) their corresponding amplification images. Insets are the Co<sub>3</sub>O<sub>4</sub> particle size distribution.

### 3.2.1. Catalytic performance in CO<sub>2</sub> methanation

Fig. 14 shows the activity and CH<sub>4</sub> selectivity of citric acid-assisted Co/ZrO<sub>2</sub> catalysts for 8 h time-on-stream (TOS). Both CO<sub>2</sub> conversion and CH<sub>4</sub> selectivity were enhanced significantly on the citric acid-assisted Co/ZrO<sub>2</sub> catalysts compared with the benchmark Co/ZrO<sub>2</sub> catalyst without citric acid for impregnation. With the increase of n<sub>CA/Co</sub> values till 2, the CO<sub>2</sub> conversion and CH<sub>4</sub> selectivity gradually increased and reached the maximum at 85% and 99%, respectively. Particularly, the CO<sub>2</sub> conversion of 2CA-2Co/ZrO<sub>2</sub> is more than twice of that with

conventional Co/ZrO<sub>2</sub> catalyst (e. g. 38%). Considering the citric acid-dependent behavior of particle size from XRD and TEM results, the catalyst activity increased with the decrease of metal particle size. However, when the n<sub>CA/Co</sub> value exceeds 2, no further enhancement is observed. Beyond this point, both CO<sub>2</sub> conversion and CH<sub>4</sub> selectivity even slightly decreased at the n<sub>CA/Co</sub> value of 5. In order to compare the stability of citric acid-assisted catalyst and the original catalyst, 300 h stability test has been conducted with 10 wt% Co loading and shown in Fig. S1. Fig. S1 reveals that both the 2CA-10Co/ZrO<sub>2</sub> and 10Co/ZrO<sub>2</sub> still exhibits superior and stable activity even after 300 h TOS. The organic acid-assisted strategy not only improves the catalytic activity but also maintains the stability.

To understand the particle size-activity relationship, metal dispersion was determined by H<sub>2</sub> titration experiment, and turnover frequency (TOF) was calculated accordingly. Table 2 shows the metal dispersion increases monotonically with the increase of n<sub>CA/Co</sub> values, whereas the TOF reaches the maximum (1116 h<sup>-1</sup>) at n<sub>CA/Co</sub> value of 2, and slightly drops with a further addition citric acid.

Evidently, the monotonical relationship between metal dispersion and TOF with the n<sub>CA/Co</sub> ranging from 0 to 2 demonstrates the importance of well dispersed metal particles in the enhancement of activity. However, an excessive of citric addition leads to a loss of activity, indicative of other factors other than particle size affecting activity. To identify the factors and their correlation with catalytic performance, the reduction behavior and surface property were examined by H<sub>2</sub>-TPR, CO<sub>2</sub>-TPD and XPS, respectively. Detailed results will be discussed in the following sections.

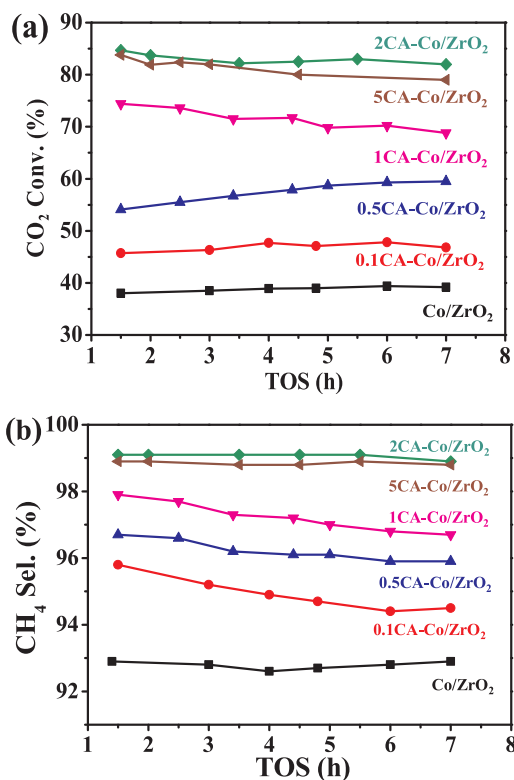


Fig. 14. (a) CO<sub>2</sub> conversion and (b) CH<sub>4</sub> selectivity over the CA-Co/ZrO<sub>2</sub> catalysts with different concentrations of citric acid in the impregnant and benchmark Co/ZrO<sub>2</sub>. Conditions: molar ratio of H<sub>2</sub>/CO<sub>2</sub> = 4/1, GHSV = 7200 ml g<sup>-1</sup> h<sup>-1</sup>, P = 3 MPa, T = 400 °C.

**Table 2**  
Characteristics of the reduced CA-2Co/ZrO<sub>2</sub> catalysts with different concentrations of citric acid in the impregnant.

n <sub>CA</sub> :n <sub>Co</sub>	Co dispersion <sup>a</sup> (%)	TOF <sup>b</sup> (h <sup>-1</sup> )	Amount of adsorbed CO <sub>2</sub> (μmol/g)
0	11.6	756	22
0.1	12.1	828	28
0.5	14.1	900	70
1	15.8	1044	105
2	17.3	1116	110
5	19.6	972	99

<sup>a</sup> Metal dispersion was determined by the H<sub>2</sub> titration analysis.

<sup>b</sup> TOF = (GHSV × 1/5/22.4 × CO<sub>2</sub> Conversion) / (metal mole × reduction degree × dispersion), and the TOF data displayed in Table 2 is corresponding to the 2 h TOS.

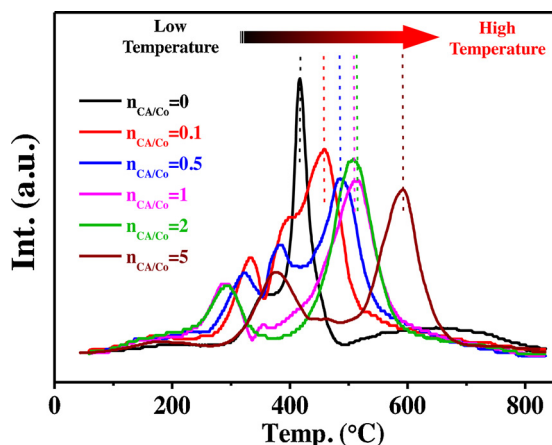


Fig. 15.  $\text{H}_2$ -TPR profiles of catalyst precursors  $\text{Co}_3\text{O}_4/\text{ZrO}_2$  with different concentrations of citric acid in the impregnation solution.

### 3.3. The reduction and adsorption capacity of catalysts

Fig. 15 shows the  $\text{H}_2$ -TPR profiles of CA- $\text{Co}_3\text{O}_4/\text{ZrO}_2$  catalyst precursors. The presence of two main reduction peaks can be observed for all catalysts. The first peak, ranged from 290–380 °C, might relate to higher mobility of surface oxygen on  $\text{ZrO}_2$  support [59–62]; the second peak, ranged from 420–600 °C, can be assigned to the reduction of  $\text{Co}_3\text{O}_4$  located on the support that has strong interaction with the  $\text{ZrO}_2$  support. The shoulder peak in the low temperature side of the second peak corresponds to free  $\text{Co}_3\text{O}_4$  species on the  $\text{ZrO}_2$  surface and the  $\text{Co}_3\text{O}_4$  located on the support but with weak interaction with  $\text{ZrO}_2$  [6,63]. Compared with  $\text{Co}_3\text{O}_4/\text{ZrO}_2$ , the first peak with CA- $\text{Co}_3\text{O}_4/\text{ZrO}_2$  catalysts shifts to relatively lower temperatures, indicating more surface oxygen species can be reduced at a lower temperature, and oxygen vacancy formation is more feasible on CA- $\text{Co}_3\text{O}_4/\text{ZrO}_2$ , especially when the  $n_{\text{CA}/\text{Co}}$  value is 2. On the other hand, the second peak of CA- $\text{Co}_3\text{O}_4/\text{ZrO}_2$  evidently shifts to higher temperatures (e.g., from 410 to 600 °C) in comparison with that of  $\text{Co}_3\text{O}_4/\text{ZrO}_2$ , implying the significantly enhanced Co- $\text{ZrO}_2$  interaction corresponding to the reduced particle size [64]. These observations are in agreement with the TEM and XRD analyses. Both the two peaks have higher  $\text{H}_2$  uptakes on the CA- $\text{Co}_3\text{O}_4/\text{ZrO}_2$  catalysts compared with  $\text{Co}_3\text{O}_4/\text{ZrO}_2$  catalysts, indicating that more oxygen vacancy and reducible metal species are available on CA- $\text{Co}_3\text{O}_4/\text{ZrO}_2$  catalysts.

$\text{CO}_2$ -TPD profiles of pre-reduced catalysts are shown in Fig. 16. The  $\text{CO}_2$  desorption occurs in three temperatures regions [65,66]: 50–150 °C, 150–250 °C and > 250 °C, which correspond to weak, medium and strong  $\text{CO}_2$  adsorption, respectively [67]. With the

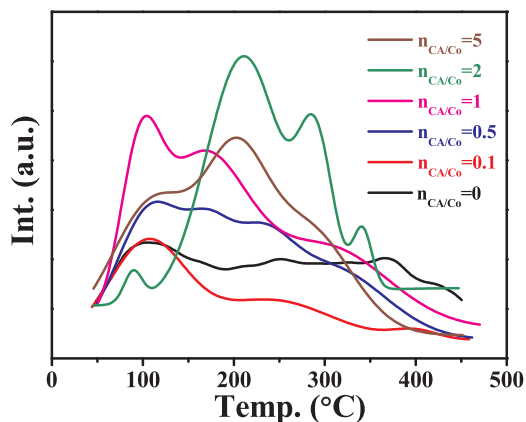


Fig. 16.  $\text{CO}_2$ -TPD profiles of CA-Co/ $\text{ZrO}_2$  catalysts with different concentrations of citric acid in the impregnant.

increasing amount of citric acid addition, not only do the medium adsorption of CA-Co/ $\text{ZrO}_2$  catalysts shift to higher temperatures, but the catalysts also display stronger adsorption towards  $\text{CO}_2$ , particularly at  $n_{\text{CA}/\text{Co}} = 2$ . Such characteristic shift in adsorption behavior is in accordance with the DFT computational results, as the  $\text{CO}_2$  adsorption at Co- $\text{ZrO}_2$  interface is more thermodynamically stable [25]. In other words, the smaller metal particle size gives rise to a large area of Co- $\text{ZrO}_2$  interface which accounts for the strongly-bonded  $\text{CO}_2$  species [24]. Interestingly, all CA-Co/ $\text{ZrO}_2$  catalysts show higher  $\text{CO}_2$  uptakes than the benchmark Co/ $\text{ZrO}_2$  catalysts, wherein 2CA-Co/ $\text{ZrO}_2$  catalyst exhibits the best  $\text{CO}_2$  adsorption capability (Table 2). Compared with the  $\text{H}_2$  dissociation and  $\text{H}^*$  migration,  $\text{CO}_2$  activation is more difficult and crucial in the  $\text{CO}_2$  hydrogenation process [25,68]. Noticeably, 2CA-Co/ $\text{ZrO}_2$  catalyst, with superior  $\text{CO}_2$  adsorption capability, displays the highest  $\text{CO}_2$  conversion and highest TOF. Clearly, well-dispersed smaller metal particles remarkably strengthen the metal-support interaction which is advantageous to the adsorption toward strongly-bonded  $\text{CO}_2$  species, making the subsequent hydrogenation more feasible. Albeit possessing the smallest particle size, 5CA-Co/ $\text{ZrO}_2$ , with even more citric acid addition, still shows a slight decrease of  $\text{CO}_2$  uptake in comparison to 2CA-Co/ $\text{ZrO}_2$ . It is possible that the smaller  $\text{Co}_3\text{O}_4$  particles in 5CA-Co/ $\text{ZrO}_2$  has excessively strong metal-support interaction as revealed from the  $\text{H}_2$ -TPR and TEM, which leads to an insufficient number of reduced active metals under the condition and a slight decrease of  $\text{CO}_2$  conversion. In addition, 5CA-Co/ $\text{ZrO}_2$  may possess the difference in the chemical state compared with 2CA-Co/ $\text{ZrO}_2$ , leading to the TOF decrease. To clarify it, the catalysts were characterized by XPS.

### 3.4. The chemical state of active sites and catalysts

As discussed in Section 3.4, a close interaction between Co metal and  $\text{ZrO}_2$  support is evidenced. Fig. 17(a) depicts the XPS spectra in the Co 2p region for reduced CA-Co/ $\text{ZrO}_2$ , and the corresponding XPS data are summarized in Table 3. The spectra of CA-Co/ $\text{ZrO}_2$  catalysts exhibit an intense peak centering at 778.8 eV, along with an additional satellite peak centering at 780.6 eV. Deconvolution analysis indicates 2CA-Co/ $\text{ZrO}_2$  exhibits the highest reduced cobalt species, whose  $\text{Co}^{2+}/\text{Co}^{3+}$  atomic ratio is 81:19. Clearly, the higher atomic ratio of  $\text{Co}^{2+}/\text{Co}^{3+}$  for 2CA-Co/ $\text{ZrO}_2$  indicates a relatively more electron-rich surface. This further implies its better reducibility, which appears to be in line with the TPR results and the explanation in Section 3.4.

Fig. 17(b) presents the XPS spectra in the O 1s region for the same samples. The intense peak at 527.8 eV can be attributed to the lattice oxygen, while the signals at 529.5 eV can be assigned to the surface hydroxyl groups or the adsorbed oxygen [69,70]. Based on the area integrals of the lattice oxygen ( $O_{\alpha}$ ) and surface hydroxyl/adsorbed oxygen ( $O_{\beta}$ ), the ratio of  $O_{\beta}$  to  $O_T$  ( $O_T = O_{\alpha} + O_{\beta}$ ) for all samples was estimated and tabulated in Table 3. The reduced 2CA-Co/ $\text{ZrO}_2$  exhibits a higher ratio of  $O_{\beta}/O_T$  than that of conventional Co/ $\text{ZrO}_2$ , implying a significant decrease of lattice oxygen  $O_{\alpha}$  on this sample. In other words, such behavior is indicative of the increasing number of oxygen vacancies on the surface upon reduction.

Fig. 17(c) depicts the XPS spectra in the Zr 3d region. Deconvolution analysis was applied to the superimposed peak of Zr 3d<sub>5/2</sub>, and the results indicate the existence of two components: one due to the  $\text{Zr}^{4+}$  with lower BEs (ca. 179.5 eV) and the other to  $\text{Zr}^{3+}$  with higher BEs (ca. 180.2 eV) [71]. The ratio of  $\text{Zr}^{3+}/(\text{Zr}^{3+} + \text{Zr}^{4+})$  was estimated using the integrals as well and tabulated in Table 3. Noticeably, the ratio of  $\text{Zr}^{3+}/(\text{Zr}^{3+} + \text{Zr}^{4+})$  increases with the citric acid addition initially, and reaches the maximum on the 2CA-Co/ $\text{ZrO}_2$ . Such volcano-like trend appears to resemble the trend of oxygen vacancy observed in O 1s photoelectron spectra. Again, such correlation corroborates the metal-support interaction between Co species and  $\text{ZrO}_2$  on the surface.

XPS results point to the more reduced cobalt species and oxygen vacancy on the CA-Co/ $\text{ZrO}_2$  catalyst compared to the conventional Co/

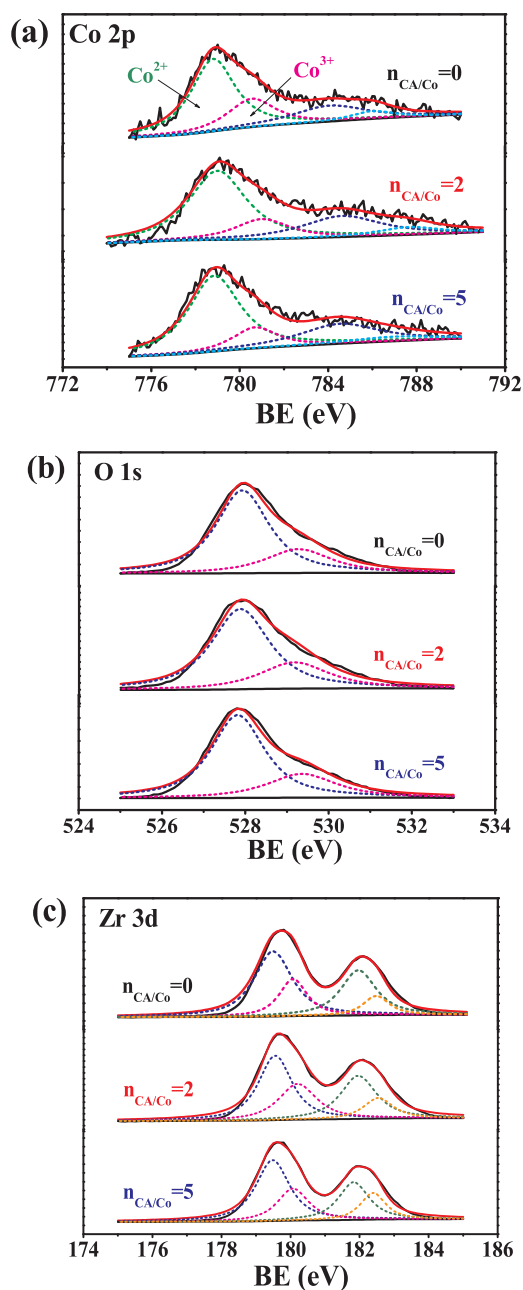


Fig. 17. XPS spectra of (a) Co 2p, (b) O 1s and (c) Zr 3d on the reduced CA-Co/ZrO<sub>2</sub> catalysts with different concentrations of citric acid in the impregnant.

Table 3

Summary of the XPS data for reduced catalyst samples.

Sample	Co <sup>2+</sup> :Co <sup>3+</sup>	O <sub>β</sub> /O <sub>T</sub> <sup>a</sup> (%)	Zr <sup>3+</sup> /(Zr <sup>3+</sup> + Zr <sup>4+</sup> ) (%)
n <sub>CA/Co</sub> =0	71:29	25.1	29.5
n <sub>CA/Co</sub> =2	81:19	27.9	38.7
n <sub>CA/Co</sub> =5	78:22	26.9	32.8

<sup>a</sup> Ratios of O<sub>β</sub> and O<sub>T</sub> were calculated from area integration of O<sub>α</sub> and O<sub>β</sub> in O 1s XPS spectra (O<sub>T</sub>=O<sub>α</sub>+ O<sub>β</sub>).

ZrO<sub>2</sub> without citric acid in preparation, and the highest oxygen vacancy concentration is reached on 2CA-Co/ZrO<sub>2</sub>. The identified oxygen vacancy on Co/ZrO<sub>2</sub> is expected to contribute to adsorbing and activating CO<sub>2</sub> [72]. In CO<sub>2</sub>-TPD profiles, the peaks at high temperature originate from desorption of CO<sub>2</sub> that interacted strongly with oxygen vacancies [73]. Therefore, the relationship between size effect, surface chemical

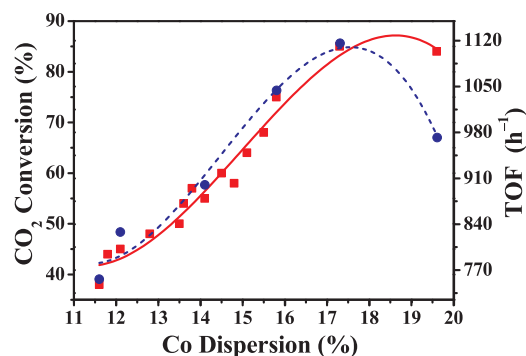


Fig. 18. The plot of CO<sub>2</sub> conversion (red solid line) and TOF (blue dash line) as a function of Co dispersion. (For interpretation of the references to colour in this figure legend, the reader is referred to the web version of this article).

property, and catalytic performance can be summarized as follows the more the reduced well-dispersed cobalt species is, the higher the oxygen vacancy concentrations are, as well as the stronger CO<sub>2</sub> adsorption capability. Superior CO<sub>2</sub> conversion and TOF would thus be expected in this way.

In summary, the organic acids-assisted strategy improves the metal dispersion and the catalytic activity of Co-ZrO<sub>2</sub> catalysts effectively. Fig. 18 is plots CO<sub>2</sub> conversion and TOF as a function of Co dispersion. The CO<sub>2</sub> conversion increased with the increasing Co dispersion, however, there was a slight decrease when the Co dispersion increased to 19.6%. Meanwhile, the TOF also increased with the Co dispersion increase seen from the blue dash line in Fig. 18. Therefore, the CO<sub>2</sub> conversion increase is associated with two aspects caused by the Co dispersion increase: 1) the increase in number of reduced Co sites; 2) the increase of the catalytic activity in terms of TOF of reduced Co sites (blue dash line in Fig. 18). The increase of TOF may be due to the increased oxygen vacancies with improved dispersion (Table 3) and Co-ZrO<sub>2</sub> interface [24] caused by the intensive metal-support interaction with decreased metal particle size. When the dispersion increased to 19.6%, the partially reduced Co species and less oxygen vacancies resulted in the decrease of CO<sub>2</sub> conversion and TOF. In general, the organic acids-assisted strategy can lead to the increase of Co dispersion on Co/ZrO<sub>2</sub> catalysts; the appropriate Co dispersion tuned by the organic acid can give more reduced Co sites with higher level of oxygen vacancy and lead to the higher catalysts activity.

#### 4. Conclusion

Many organic acids with different molecular weight, carboxyl, hydroxyl and amino groups were applied to prepare highly dispersed Co catalysts supported on ZrO<sub>2</sub> with low metal loading at 2 wt.% for CO<sub>2</sub> methanation. Among the acids examined, the carboxylic acid with longer chain or larger steric hindrance, more carboxyl groups and hydroxyl groups is the better choice. Furthermore, the amino acids can also change the charge property of ZrO<sub>2</sub> surface through controlling the solution pH and increase the metal dispersion through strong electrostatic adsorption.

Among the various organic acids, citric acid-assisted Co-ZrO<sub>2</sub> catalyst shows the best catalytic performance. Evidenced by TEM, FT-IR and XRD, the forming of a cobalt citrate complex used as a Co precursor facilitates the Co dispersion on support and strengthens the Co-ZrO<sub>2</sub> interaction. Such intensified Co-ZrO<sub>2</sub> interaction in turn gives rise to more oxygen vacancies and CO<sub>2</sub> adsorption. Metal dispersion increased and particle size decreased with n<sub>CA/Co</sub> values increasing from 0 to 5. Albeit possessing the smallest particle size, 5CA-Co/ZrO<sub>2</sub>, still shows a slight decrease of CO<sub>2</sub> uptake and oxygen vacancy in comparison to 2CA-Co/ZrO<sub>2</sub>. When the n<sub>CA/Co</sub> values increased to 2, the CO<sub>2</sub> conversion and CH<sub>4</sub> selectivity increased up to the maximum 85% and 99%, respectively, and exhibited the highest TOF 1116 h<sup>-1</sup>. Evidently,

the linear relationship between metal dispersion and TOF with the  $n_{\text{Co}}/c_{\text{Co}}$  ranging from 0 to 2 demonstrates the importance of well dispersed metal particles in the enhancement of activity. However, the existence of high dispersion metal sites is not the only unique factor for the CO<sub>2</sub> methanation catalysts. It is apparent that the chemical structure of the Co species is pivotal in the CO<sub>2</sub> methanation. Appropriate Co metal-ZrO<sub>2</sub> support interaction leads to more reduced active sites and more oxygen vacancies, thus giving more CO<sub>2</sub> adsorption and high catalytic activity.

In general, the organic acids-assisted strategy can lead to significantly increased Co dispersion on Co/ZrO<sub>2</sub> catalysts; the appropriate metal dispersion tuned by the organic acid amount can give the suitable chemical state of Co species and finally lead to the higher catalysts activity.

The organic acid-assisted versatile strategy provides a new design approach for highly dispersed and active catalysts and the fundamental understanding on the chemical state of Co species provides new insights into the key factors affecting activity of CO<sub>2</sub> hydrogenation catalysts.

### Acknowledgements

This work was financially supported by the National Key Research and Development Program of China (No. 2016YFB0600902-5) and the National Natural Science Foundation of China (No. 21503029).

### Appendix A. Supplementary data

Supplementary material related to this article can be found, in the online version, at doi:<https://doi.org/10.1016/j.apcatb.2019.05.028>.

### References

- [1] B. Kahn, *Scientific American*, April 21 (2017).
- [2] B. Mutz, H.W.P. Carvalho, S. Mangold, W. Kleist, J.D. Grunwaldt, *J. Catal.* 327 (2015) 48–53.
- [3] W. Li, H. Wang, X. Jiang, J. Zhu, Z. Liu, X. Guo, C. Song, *RSC Adv.* 8 (2018) 7651–7669.
- [4] C. Galletti, S. Specchia, G. Saracco, V. Specchia, *Chem. Eng. Sci.* 65 (2010) 590–596.
- [5] J. Janlamool, P. Praserttham, B. Jongsomjit, *J. Nat. Gas Chem.* 20 (2011) 558–564.
- [6] G. Zhou, T. Wu, H. Xie, X. Zheng, *Int. J. Hydrogen Energy* 38 (2013) 10012–10018.
- [7] G. Zhou, T. Wu, H. Zhang, H. Xie, Y. Feng, *Chem. Eng. Commun.* 201 (2014) 233–240.
- [8] H. Shin, L. Lu, Z. Yang, C. Kiely, S. McIntosh, *ACS Catal.* 6 (2016) 2811–2818.
- [9] G. Du, S. Lim, Y. Yang, C. Wang, L. Pfeifferle, G. Haller, *J. Catal.* 249 (2007) 370–379.
- [10] I. Rossetti, C. Biffi, C. Bianchi, V. Nichele, M. Signoretto, F. Menegazzo, E. Finocchio, G. Ramis, A. Di Michele, *Appl. Catal. B: Environ.* 117–118 (2012) 384–396.
- [11] D. Theleritis, S. Souentie, A. Siokou, A. Katsaounis, C.G. Vayenas, *ACS Catal.* 2 (2012) 770–780.
- [12] J. Kwak, L. Kovarik, J. Szanyi, *ACS Catal.* 3 (2013) 2449–2455.
- [13] A. Karelovic, P. Ruiz, *Appl. Catal. B: Environ.* 113–114 (2012) 237–249.
- [14] J. Park, E. McFarland, *J. Catal.* 266 (2009) 92–97.
- [15] J. Kwak, L. Kovarik, J. Szanyi, *ACS Catal.* 3 (2013) 2094–2100.
- [16] J. Liu, D. Cui, J. Yu, F. Su, G. Xu, *Chin. J. Chem. Eng.* 23 (2015) 86–92.
- [17] R. Razaq, C. Li, M. Usman, K. Suzuki, S. Zhang, *Chem. Eng. J.* 262 (2015) 1090–1098.
- [18] M. Aziz, A. Jalil, S. Triwahyono, R. Mukti, Y. Taufiq-Yap, M. Sazegar, *Appl. Catal. B: Environ.* 147 (2014) 359–368.
- [19] Z. Wang, Z. Xu, S. Peng, M. Zhang, G. Lu, Q. Chen, Y. Chen, G. Guo, *ACS Catal.* 5 (2015) 4255–4259.
- [20] G. Johnson, A. Bell, *ACS Catal.* 6 (2016) 100–114.
- [21] N. Shimoda, D. Shoji, K. Tani, M. Fujiwara, K. Urasaki, R. Kikuchi, S. Satokawa, *Appl. Catal. B: Environ.* 174 (2015) 486–495.
- [22] G. Zeng, J. Qiu, Z. Li, P. Pavaskar, S. Cronin, *ACS Catal.* 4 (2014) 3512–3516.
- [23] D. Upham, A. Derk, S. Sharma, H. Metiu, E. McFarland, *Catal. Sci. Technol.* 5 (2015) 1783–1791.
- [24] W. Li, X. Nie, X. Jiang, A. Zhang, F. Ding, M. Liu, Z. Liu, X. Guo, C. Song, *Appl. Catal. B: Environ.* 220 (2018) 397–408.
- [25] X. Nie, H. Wang, W. Li, Y. Chen, X. Guo, C. Song, *J. CO<sub>2</sub> Util.* 24 (2018) 99–111.
- [26] H. Wu, Y. Chang, J. Wu, J. Lin, I. Lin, C. Chen, *Catal. Sci. Technol.* 5 (2015) 4154–4163.
- [27] J. Matsubu, V. Yang, P. Christopher, *J. Am. Chem. Soc.* 137 (2015) 3076–3084.
- [28] V. Iablokov, S. Beaumont, S. Alayoglu, V. Pushkarev, C. Specht, J. Gao, A. Alivisatos, N. Kruse, G. Somorjai, *Nano Lett.* 12 (2012) 3091–3096.
- [29] S. Sokolov, E. Kondratenko, M. Pohl, A. Barkschat, U. Rodemerck, *Appl. Catal. B: Environ.* 113–114 (2012) 19–30.
- [30] V. Nichele, M. Signoretto, F. Menegazzo, A. Gallo, V. Dal Santo, G. Cruciani, G. Cerrato, *Appl. Catal. B: Environ.* 111–112 (2012) 225–232.
- [31] A. Abdel-Mageed, D. Widmann, S. Olesen, I. Chorkendorff, J. Biskupek, R. Behm, *ACS Catal.* 5 (2015) 6753–6763.
- [32] S. Li, Y. Xu, Y. Chen, W. Li, L. Lin, M. Li, Y. Deng, X. Wang, B. Ge, C. Yang, S. Yao, J. Xie, Y. Li, X. Liu, D. Ma, *Angew. Chem. Int. Ed.* 56 (2017) 1–6.
- [33] F. Che, S. Ha, J.S. McEwen, *Angew. Chem. Int. Ed.* 56 (2017) 3557–3561.
- [34] P. Li, A. Aijaz, Q. Xu, *Angew. Chem. Int. Ed.* 51 (2012) 6753–6756.
- [35] F. Westerhaus, R. Jagadeesh, G. Wienhöfer, M. Pohl, J. Radnik, A. Surkus, J. Rabeah, K. Junge, H. Junge, M. Nielsen, A. Brückner, M. Beller, *Nat. Chem.* 5 (2013) 537.
- [36] W. Li, A. Zhang, X. Jiang, C. Chen, Z. Liu, C. Song, X. Guo, *ACS Sus. Chem. Eng.* 5 (2017) 7824–7831.
- [37] J. Liu, A. Zhang, M. Liu, S. Hu, F. Ding, C. Song, X. Guo, *J. CO<sub>2</sub> Util.* 21 (2017) 100–107.
- [38] T. Fujikawa, K. Masahiro, T. Ebihara, K. Hagiwara, T. Kubota, Y. Okamoto, *J. Jpn. Petrol. Inst.* 48 (2005) 114–120.
- [39] W. Li, H. Huang, H. Li, W. Zhang, H. Liu, *Langmuir* 24 (2008) 8358.
- [40] G. Jacobs, J.A. Chaney, P.M. Patterson, T.K. Das, B.H. Davis, *Appl. Catal. A Gen.* 264 (2004) 203–212.
- [41] S. Vada, A. Hoff, E. Adnanes, D. Schanke, A. Holme, *Top. Catal.* 2 (1995) 155–162.
- [42] A. Pimerzin, A. Mozhaev, A. Varakin, K. Maslakov, P. Nikulshin, *Appl. Catal. B: Environ.* 205 (2017) 93–103.
- [43] H. Li, M. Li, Y. Chu, F. Liu, H. Nie, *Appl. Catal. A Gen.* 403 (2011) 75–82.
- [44] B. Jongsomjit, J. Panpranot, J. Goodwin, *J. Catal.* 204 (2001) 98–109.
- [45] E. Köck, M. Kogler, T. Götsch, L. Schlicker, M. Bekheet, A. Gurlo, A. Doran, B. Kloetzer, B. Petermüller, D. Schildhammer, N. Yigit, S. Penner, *Dalton Trans.* 46 (2017) 4554–4570.
- [46] K. Karwacki, P. Ganesh, P. Kent, W. Gordon, G. Peterson, J. Niu, Y. Gogotsi, *J. Mater. Chem. A* 1 (2013) 6051–6062.
- [47] G. Veith, A. Lupini, S. Pennycook, N. Dudney, *ChemCatChem* 2 (2010) 281–286.
- [48] A. Gabriel, M. Veith, N. Dudney, *J. Phys. Chem. C* 113 (2009) 269–280.
- [49] M. Jensen, K. Venkataramani, S. Helveg, B. Clausen, M. Reichling, F. Besenbacher, J. Lauritsen, *J. Phys. Chem. C* 112 (2008) 16953–16960.
- [50] M. Hisamoto, R. Nelson, M. Lee, J. Eckert, S. Scott, *J. Phys. Chem. C* 113 (2009) 8794–8805.
- [51] J. Sun, J. Zhang, H. Fu, H. Wan, Y. Wan, X. Qu, Z. Xu, D. Yin, S. Zheng, *Appl. Catal. B: Environ.* 229 (2018) 32–40.
- [52] L. Jiao, J. Regalbuto, *J. Catal.* 260 (2008) 342–350.
- [53] L. Jiao, J. Regalbuto, *J. Catal.* 260 (2008) 329–341.
- [54] B. Mehrabadi, S. Eskandari, U. Khan, R. White, J. Regalbuto, *Adv. Catal.* 61 (2017) 1–35.
- [55] L.F. Diniz, M.S. Souza, P.S. Carvalho, C.C.P. da Silva, R.F. D’Vries, J. Elena, J. Mol. Struct. 1153 (2018) 58–68.
- [56] K. Hoda, M. Sudolska, S. Kalytchuk, D. Nachtigalova, A.L. Rogach, M. Otyepka, R. Zboril, *ACS Nano* 11 (2017) 12402–12410.
- [57] H. Singh, J.K. Rajput, *J. Mater. Sci.* 53 (2017) 3163–3188.
- [58] N. Ilić, A. Džunuzović, J. Bobić, B. Stojadinović, P. Hammer, M. Vijatović Petrović, Z. Dohčević-Mitrović, B. Stojanović, *Ceram. Int.* 41 (2015) 69–77.
- [59] P. Schmidt, T. Rosenband, C. Langer, W. Itano, J. Bergquist, D. Wineland, *Science* 309 (2005) 749–752.
- [60] C. Campbell, C. Peden, *Science* 309 (2005) 713–714.
- [61] Y. Namai, K. Fukui, Y. Iwasawa, *J. Phys. Chem. B* 107 (2003) 11666–11673.
- [62] Y. Namai, K. Fukui, Y. Iwasawa, *Catal. Today* 85 (2003) 79–91.
- [63] J. Zhang, J. Chen, J. Ren, Y. Li, Y. Sun, *Fuel* 82 (2003) 581–586.
- [64] Y. Liu, K. Fang, J. Chen, Y. Sun, *Green Chem.* 9 (2007) 611–615.
- [65] H. Wang, M. Wang, W. Zhang, N. Zhao, W. Wei, Y. Sun, *Catal. Today* 115 (2006) 107–110.
- [66] V.K. Díez, C.R. Apestequía, J.I. Di Cosimo, *Catal. Today* 63 (2000) 53–62.
- [67] C. Zhong, X. Guo, D. Mao, S. Wang, G. Wu, G. Lu, *RSC Adv.* 5 (2015) 52958–52965.
- [68] X. Nie, H. Wang, M.J. Janik, Y. Chen, X. Guo, C. Song, *J. Phys. Chem. C* 121 (2017) 13164–13174.
- [69] J. Zhu, J. Yang, Z.F. Bian, J. Ren, Y.M. Liu, Y. Cao, H.X. Li, H.Y. He, K.N. Fan, *Appl. Catal. B: Environ.* 76 (2007) 82–91.
- [70] Z. He, W. Que, J. Chen, Y. He, G. Wang, *J. Phys. Chem. Solids* 74 (2013) 924–928.
- [71] H. Li, J. Ren, X. Qin, Z. Qin, J. Lin, Z. Li, *RSC Adv.* 5 (2015) 96504–96517.
- [72] X. Liu, M. Wang, C. Zhou, W. Zhou, K. Cheng, J. Kang, Q. Zhang, W. Deng, Y. Wang, *Chem. Comm.* 54 (2018) 140–143.
- [73] P. Gao, S. Dang, S. Li, X. Bu, Z. Liu, M. Qiu, C. Yang, H. Wang, L. Zhong, Y. Han, Q. Liu, W. Wei, Y. Sun, *ACS Catal.* 8 (2017) 571–578.